Mechanisms of barrier layer formation and erosion from in situ observations in the Bay of Bengal

Jenson V. George

Centre for Atmospheric and Oceanic Sciences, Indian Institute of Science, Bangalore,

India

P.N. Vinayachandran [*]

Centre for Atmospheric and Oceanic Sciences, Indian Institute of Science, Bangalore,

India

V. Vijith

Cochin University of Science and Technology, Cochin, India

V. Thushara

Centre for Atmospheric and Oceanic Sciences, Indian Institute of Science, Bangalore,

India

Anoop A. Nayak

Centre for Atmospheric and Oceanic Sciences, Indian Institute of Science, Bangalore,

India

Shrikant M. Pargaonkar

Centre for Atmospheric and Oceanic Sciences, Indian Institute of Science, Bangalore,

India

P. Amol

National Institute of Oceanography, Regional Centre, Visakhapatnam, India

K. Vijaykumar

National Institute of Oceanography, Goa, India

Adrian J. Matthews

Centre for Ocean and Atmospheric Sciences, School of Environmental Sciences and

School of Mathematics, University of East Anglia, Norwich, UK

[*]*Corresponding author address:* P.N. Vinayachandran, Centre for Atmospheric and

Oceanic Sciences, Indian Institute of Science, Bangalore 560012, India

E-mail: vinay@iisc.ac.in

ABSTRACT

During the Bay of Bengal (BoB) Boundary Layer Experiment (BoBBLE) in the southern BoB, time series of microstructure measurements were obtained at 8°N, 89°E from 4–14 July, 2016. These observations captured events of barrier layer (BL) erosion and re-formation. Initially, a three-layer structure was observed: a fresh surface mixed layer (ML) of thickness 10–20 m; a BL below of 30–40 m thickness with similar temperature but higher salinity; a high salinity core layer, associated with Summer Monsoon Current. Each of these three layers was in relative motion to the others, leading to regions of high shear at the interfaces. However, haline stratification overcame the destabilizing influence of the shear regions, and preserved the three-layer structure. A salinity budget using in-situ observations suggested that during the BL erosion, high salinity surface waters (34.5 PSU) with weak stratification were advected to the time series location and replaced the three–layer structure with a deep ML (~60 m). Weakened stratification at the time series location also allowed atmospheric wind forcing to penetrate deeper. Turbulent kinetic energy dissipation rate and eddy diffusivity showed elevated values above 10^{-7} W kg^{-1} and 10^{-4} m^2 s^{-1}, respectively, in the upper 60 m. Later, the surface salinity decreased again (33.8 PSU) through horizontal advection, stratification became stronger and elevated mixing rates were confined to the upper 20 m, and the BL re-formed. A 1D model analysis suggests that in the study region, advection of temperature-salinity characteristics is essential for the maintenance of BL and to the extent to which mixing penetrates the water column.

3

1. Introduction

The Bay of Bengal (BoB) is a semi-enclosed sea in the North Indian Ocean characterized by strong surface layer stratification (Shetye et al. 1991, 1996; Shenoi et al. 2002). The strongest stratification occurs during the summer monsoon in the northern BoB where heavy rainfall and river influx result in a low salinity surface layer (Vinayachandran et al. 2002; Rao and Sivakumar 2003; MacKinnon et al. 2016). In contrast to the northern BoB, the southern BoB receives less rainfall and therefore surface salinity is higher (Matthews et al. 2015; Das et al. 2016). The Summer Monsoon Current (SMC) flowing from the Arabian Sea to the south of Sri Lanka carries high salinity water to the southern BoB (Murty et al. 1992; Vinayachandran et al. 1999; Jensen 2003; Webber et al. 2018). Arabian Sea High Salinity Water (ASHSW) entering the southern BoB subducts below the BoB surface water and flows northward. This subducted ASHSW creates a subsurface salinity maximum in the upper thermocline region (Vinayachandran et al. 2013; Jain et al. 2017).

A strong halocline associated with the presence of a freshened surface layer over a saline subsurface layer results in the formation of a barrier layer (Lukas and Lindstrom (1991); Vinayachandran et al. (2002); Thadathil et al. (2007); Sengupta and Ravichandran (2001)). The barrier layer is defined as the region between the mixed layer depth (MLD) and the isothermal layer depth. The barrier layer forms because of the salinity induced stratification, and is observed in many parts of the world ocean (Lukas and Lindstrom 1991; Sprintall and Tomczak 1992; You 1995; Kara et al. 2000; de Boyer Montégut et al. 2007; Mignot et al. 2007; Durand et al. 2007). When a barrier layer is present, the water entrained into the mixed layer originates from the isothermal

layer and the SST of the mixed layer is not affected. Barrier layer formation and decay are important for climate as they regulate the intra-seasonal oscillations of the monsoon (Thadathil et al. 2016; Li et al. 2017). The barrier layer controls the heat budget of the mixed layer by acting as a barrier for the penetration of surface forcing to the deeper layer (Shenoi et al. 2002; Akhil et al. 2014; Chowdary et al. 2015). The barrier layer also plays a significant role in the intensification of tropical cyclones (Balaguru et al. 2012; Yan et al. 2017), and regulates chlorophyll blooms as it acts as a barrier to nutrient supply (Vidya et al. 2017).

Among the barrier layers observed in the tropical oceans, one of the most frequent and thickest occurs in the northern BoB (de Boyer Montégut et al. 2007; Mignot et al. 2007). Owing to the large salinity gradient between the surface layer and the top of the thermocline, the stratification in the barrier layer of the northern BoB is also one of the strongest (Shetye et al. 1996; Maes and O'Kane 2014; MacKinnon et al. 2016). In the southern BoB, especially the eastern part, barrier layer formation is relatively weaker (Girishkumar et al. 2011; Thangaprakash et al. 2016; Vinayachandran et al. 2018).

Despite its importance, studies of barrier layer formation and decay using in situ measurements of mixing are sparse and mostly limited to rain induced stratification in the surface layer (Smyth et al. 1997; Callaghan et al. 2014; Drushka et al. 2016). A major reason for this is the lack of direct turbulence and mixing observations, particularly in the BoB. In the BoB, measurements of vertical mixing have been made in the north (Lucas et al. 2016; Mahadevan et al. 2016) and near Sri Lanka (Jinadasa et al. 2016). Here we present micro-structure measurements that captured the erosion of the barrier layer and its re-formation during a 10-day time series in the southern BoB during the summer monsoon of 2016. The data have been used to understand the characteristics of mixing

5

in the barrier layer, and the mechanism of barrier layer formation and erosion. Our data suggest that the advection of high salinity surface waters by the SMC to the southern BoB has an important role in the barrier layer erosion.

The paper is organized as follows: The measurements and methodologies are described in Section 2. Observations of barrier layer formation and erosion are presented in Section 3. Formation mechanisms of the barrier layer and its turbulent characteristics are addressed in Section 4. Section 5 details the mechanism of barrier layer erosion. A 1D model analysis is presented in Section 6. The summary and conclusions of the present study are given in Section 7.

2. Methods and field campaign

The Bay of Bengal Boundary Layer Experiment (BoBBLE; Vinayachandran et al. (2018)) was carried out onboard ORV Sindhu Sadhana from 25 June to 24 July, 2016 in the southern BoB. The field campaign included 10 days of time series observations at 8°N, 89°E from 4–14 July, 2016 (Fig. 1). The time series location was near to the RAMA (Research Moored Array for African-Asian-Australian Monsoon Analysis and Prediction) mooring at 8°N, 89°E in the southern BoB. During the time series, a loosely tethered vertical micro-structure profiler (VMP250, Make: Rockland Scientific, Canada) was used, and profiles were measured at local time 5 AM, 9 AM, 1 PM, 5:30 PM and 11:30 PM each day down to a depth of 250 m. Each VMP250 station consisted of 2 to 3 successive profiles with an interval of 15 minutes. The VMP250 was equipped with two airfoil shear probes and standard oceanographic conductivity and temperature sensors (CT, JFE Advantech). The shear probes measure high frequency horizontal velocity fluctuations, which were further processed for estimating the local turbulent kinetic en-

ergy (TKE) dissipation rate (ε) following the standard processing technique assuming isotropic turbulence (Roget et al. 2006). The representative profile of temperature, salinity, and ε at each VMP250 station was obtained by averaging all the respective profiles at each station. These temperature, salinity profiles were binned to 1 m depth and ε profiles were binned to 3 m. Because of the significant generation of artificial turbulence by the ship, ε in the upper 10 m were removed.

Diapycnal diffusivity was calculated using the Osborn (1980) relation, $K_\rho = \Gamma \varepsilon / N^2$. Here mixing efficiency Γ was taken as a constant (0.2) following Gregg et al. (2018). This value facilitates the comparison with previous studies (e.g. Waterhouse et al. (2014)). Squared buoyancy frequency (Brunt Vaisala Frequency, N^2) is calculated as $N^2 = \frac{-g}{\rho} \frac{\partial \rho}{\partial z}$, where g is acceleration due to gravity, ρ is the observed density of sea water calculated using the station averaged temperature and salinity profiles, and z is the depth. To understand the relative contribution of temperature and salinity to stratification, N^2 can be decomposed as sum of the thermal (N_T^2) and haline (N_S^2) stratification, $N^2 = N_T^2 + N_S^2 = g\alpha \frac{\partial T}{\partial z} - g\beta \frac{\partial S}{\partial z}$ (Maes and O'Kane 2014), where T is temperature, S is salinity, and α and β are thermal expansion and haline contraction coefficients respectively. The diapycnal salt flux is calculated as $J_s = \rho K_\rho \frac{\partial S}{\partial z} \times 1000$, in mg m^{-2} s^{-1}.

In order to attain a larger view of background hydrography during the time series observations, westward and southward sections were made using an Ocean Science Underway CTD (uCTD) from the time series location every evening (Fig. 1 inset). The uCTD was equipped with SBE (Sea Bird Electronics) temperature and salinity sensors. Post processing of uCTD data was done following Ullman and Hebert (2014), and binned the temperature-salinity profiles to 1 m. The sections covered roughly 10 km, and consisted of 6–7 nearly equally spaced profiles of temperature and salinity. Current velocities

7

were measured using a vessel-mounted 150 kHz Teledyne RDI Ocean Surveyor acoustic Doppler current profiler (ADCP) during the cruise. Richardson number is defined as, $Ri = N^2/S^2$, where vertical shear is $S^2 = u_z{}^2 + v_z{}^2$, u and v are zonal and meridional velocity components, and subscript z represents the vertical gradient. Representative profiles of current vectors at each station were obtained by averaging the 2 m binned u, v profiles for the vertical microstructure profiler observation period, which was roughly 45 minutes. The shear was calculated using station averaged u, v profiles and interpolated to the depth of N^2 profiles to get the Ri.

The MLD was calculated as the depth where the density is equal to the sea surface density plus an increment in density equivalent to 0.8°C (Kara et al. 2000; Girishkumar et al. 2011; Thangaprakash et al. 2016). The isothermal layer is defined as the depth where the temperature is 0.8°C less than SST, and the barrier layer is the layer between the base of the isothermal layer and the base of the mixed layer. This definition of the isothermal layer ensures that in the absence of haline stratification, the MLD and isothermal layer depth are identical. Data from an automated weather station (AWS) installed on-board was used to compute the atmospheric fluxes following the Coupled Ocean-Atmosphere Response Experiment (COARE) 3.0 algorithm (Fairall et al. 2003).

Salinity budget of upper 60 m is attempted using insitu observations. Following Feng et al. (1998), vertically integrating the salinity tendency equation (assuming no horizontal mixing) from a fixed depth h to surface gives the form $\int_{-h}^{0} \frac{\partial S}{\partial t} dx = -\int_{-h}^{0} (\mathbf{u}.\nabla S + w\frac{\partial S}{\partial z}) dz - S_0(P-E) - K_\rho \frac{\partial S}{\partial z}$, where S is the salinity and $\mathbf{u} = (u,v)$ the horizontal velocity, h is the depth of the lower boundary (60 m), x is positive eastward, y is positive northward and z is positive upward. u, v, and w are zonal, meridional, and vertical velocities, respectively. E the evaporation, P the precipitation, and S_0 is the surface salinity.

8

All upward fluxes are positive. The left hand side (LHS) of the equation represents the salinity tendency. First term in the right hand side (RHS) of the equation represents three-dimensional advection and second term is the surface fluxes. The third term on the RHS represent vertical turbulent transport. Vertical velocity w is calculated assuming adiabatic motion in the density equation $w\frac{\partial \rho}{\partial z} = -\frac{\partial \rho}{\partial t} - u\frac{\partial \rho}{\partial x} - v\frac{\partial \rho}{\partial y}$. In the mixed layer w is considered to be linearly decreasing to zero at the surface. All the spatial and temporal gradients of salinity/density were estimated using the linear fit of daily uCTD sections and time series VMP250 observations, respectively. Details of the estimation of each terms in the salinity budget equation are given in the Appendix.

Surface currents from OSCAR (Ocean Surface Current Analysis Real-time, Lagerloef et al. (2002)) and satellite derived sea surface salinity from SMAP (Soil Moisture Active Passive, Entekhabi et al. (2010)) mission were also used to quantify the advection of high/low salinity surface waters in to the study region.

3. Observations

a. Background

The BoB during the summer monsoon is typically characterized by intraseasonal oscillations in winds and SST (Sengupta and Ravichandran 2001). The time series observations in BoBBLE were carried out during a suppressed phase of the boreal summer intraseasonal oscillation (BSISO; Lee et al. (2013)). There was no rainfall during the time series, and winds were steady southwesterlies with weak to moderate wind speed. Further details of the atmospheric conditions during BoBBLE can be found in Vinay-achandran et al. (2018).

9

The principal feature of circulation in the southern BoB during the period of observation (4–14 July, 2016) was the presence of a fully developed SMC, with speeds of 0.5 to 1 m s^{-1} (Fig. 1), carrying high salinity water from the Arabian Sea to the southern BoB. The SMC appeared as an eastward current south of Sri Lanka, and as it entered the BoB, it took a northeastward path. The SMC further forked into two main eastward branches, first at 6°N, 87°E and then at 8°N, 87°E, while the main core proceeded northwestward and fed an anticyclonic eddy centered at 10°N, 87°E. The time series location was located at a relatively quiescent region to the east of the core of the SMC with the mean surface current being southeastward (Fig. 1 inset). The SMAP surface salinity suggests that the time series location was surrounded by relatively low saline waters ($<$34 PSU), except towards the southeast and northwest where it was approximately 34.5 PSU.

b. Thermohaline variability

In this section, the basic temporal variability of the thermohaline structure of the upper layers during the observational period is presented. The time–depth section of salinity (Fig. 2b) shows two freshening events (4–5 July and 10–14 July, 2016) separated by a salinisation event (6–9 July, 2016). During the freshening events, a cooler ($<$ 29°C; Fig. 2a) and saline ($>$ 34 PSU) subsurface layer was capped by an approximately 20 m thick surface layer of less saline ($<$ 34 PSU) and warmer ($>$ 29°C) water. The MLD was confined to the base of the low salinity surface layer during both the freshening events. However, the isothermal layer penetrated to 60 m, the depth of the ˜35 PSU isohaline. The deeper isothermal layer and shallow mixed layer resulted in the formation of a barrier layer of 30–40 m thickness. During the salinisation event, the surface salinity increased from 33.84 to 34.35 over two days (from 05 July 6 PM to 07 July 1 PM, 2016

10

local time). The event was accompanied by an increase in MLD from 20 m to 60 m
and barrier layer erosion. The eroded barrier layer then reformed as the surface salinity
decreased from 34.35 to 33.8 PSU during the period 7–10 July, 2016, associated with
the MLD shallowing from 60 m to 20 m. Overall, the periods of barrier layer erosion
at the time series location were characterized by both salinisation and deepening of the
mixed layer. On the other hand, when a prominent barrier layer was present, surface
waters were less saline, and the MLD was shallow.

The time–depth section of density (Fig. 2c) shows that the presence of the low salinity
surface layer during the freshening events resulted in density stratification. This is quan-
tified by N^2 (Fig. 2d), which depicted two maxima: one at the base of the low salinity
surface layer, and the other at the base of the barrier layer. However, during the erosion
of the barrier layer, there was only one stratification maximum, at 60 m. The N^2 maxi-
mum noted at the base of the barrier layer is associated with the subsurface high salinity
core (Fig. 2b).

c. Currents

Here, the observed velocity structure is discussed in relation to the thermohaline layers
presented in section 3b. The ADCP currents during the time series showed both tem-
poral and spatial variability (Fig. 3a). In the upper mixed layer (10–20 m), the currents
were northward until 6 July, and then the direction of the flow changed to predomi-
nantly southeastward till the end of time series. In the beginning of the barrier layer
erosion (6–7 July, 2016), flow was weakly eastward, being in transition from northward
to southeastward. The time series average of the upper mixed layer ADCP currents was
southeastward, consistent with OSCAR currents (Fig. 1). In general, the flow in the bar-

11

rier layer was northeastward, but below the barrier layer, it was southwestward. Hence, there were clear current regimes corresponding to the thermohaline layers described in section 3b, indicating the possible importance of advection in the formation and erosion of the barrier layer.

Vertical shear also showed two maxima, one at the base of mixed layer and another at the base of the barrier layer (Fig. 3b), consistent with the N^2 maxima (Fig. 2d). A necessary condition for the destabilization of a stratified water column by vertical shear is that $Ri < 0.25$ (Drazin and Reid 2004). Ri showed values <0.25 in the mixed layer (the cyan dotted region in the Fig. 3 b) and at the base of the barrier layer. Occasional patches of Ri<0.25 were also noticed in the barrier layer, especially on 5, 10 and 13 July, 2016.

d. Diapycnal mixing and salt flux

The ε and K_ρ profiles revealed four distinct vertical regimes in the upper 150 m, viz., the mixed layer, the barrier layer, the barrier layer base and below the barrier layer (Fig. 4a,b). In the mixed layer, enhanced turbulent mixing was observed, with $\varepsilon > 10^{-7}$ W kg^{-1} and $K_\rho > 10^{-3}$ m^2 s^{-1}. The Highest values of ε (10^{-4} W kg^{-1}) and K_ρ (10^{-2} m^2 s^{-1}) were observed close to the surface. Below the MLD, within the barrier layer, ε and K_ρ diminished to background values of 10^{-9} W kg^{-1} and 10^{-5} m^2 s^{-1}, respectively. Occasional local maximua in ε ($>10^{-8}$ W kg^{-1}) and K_ρ ($> 10^{-4}$ m^2 s^{-1}) were noticed at the base of the barrier layer. Below the barrier layer, ε and K_ρ reduced to 10^{-9} W kg^{-1} and 10^{-6} m^2 s^{-1}, respectively. Over the course of the time series, below the barrier layer, occasional patches of ε and K_ρ with values of the order of 10^{-8} W kg^{-1} and 10^{-4} m^2 s^{-1} respectively, were also observed. This is consistent with our understanding that

12

turbulent mixing in the thermocline is characterized by intermittent, sporadic and highly transient mixing events (Fig. 4a, b; Moum et al. (1989); Thorpe (2007)).

The time series of ε and K_ρ (Fig. 4a, b) also captured the mixing event (6–9 July, 2016), where the elevated ε ($> 10^{-7}$ W kg^{-1}), and K_ρ ($> 10^{-3}$ m^2 s^{-1}) penetrated as deep as 60 m when the barrier layer eroded. The presence of high ε and K_ρ during the erosion of the barrier layer suggests that surface forcing penetrated to deeper layer.

The diapycnal salt flux J_s was calculated using the vertical salinity gradient (Fig. 4c) and K_ρ (Fig. 4b), and was generally upward ($J_s > 0$) above the isothermal layer (Fig. 4d). However, it was downward ($J_s < 0$, the cyan dotted region in Fig. 4d) below the isothermal layer due to the negative salinity gradient associated with the high salinity core (Fig. 4c). The J_s followed a pattern similar to ε, with elevated values ($> 10^1$ mg m^{-2} s^{-1}) in the mixed layer and occasional patches of J_s with value ~$10^{0.5}$ mg m^{-2} s^{-1} at the base of mixed layer and barrier layer. Within the barrier layer, J_s was in general ~10^{-1} mg m^{-2} s^{-1}, and below the barrier layer it further reduced to ~10^{-2} mg m^{-2} s^{-1}. During the barrier layer erosion, elevated J_s ($> 10^1$ mg m^{-2} s^{-1}) penetrated up to 60 m and tried to dilute the strong salinity gradient at the mixed layer base.

e. Surface forcing

Wind and buoyancy forcings are major sources of turbulence in the upper layer of the ocean (Moum and Smyth 2001). Hence, these are potential mechanisms to account for the observed evolution of the barrier layer. During the time series observations, wind speed was weak to moderate (4–11 m s^{-1}), typical of the southern BoB during the suppressed phase of BSISO. Wind stress increased (0.025 N m^{-2}–0.2 N m^{-2}) from the beginning of time series to 10 July, and then decreased to 0.025 N m^{-2} by the end

13

of the observation period (Fig. 5a). The peak in wind stress was observed on 10 July, whereas maximum MLD occurred on 7 July (Fig. 4a), and MLD decreased thereafter, associated with the re-freshening of the surface layer. The energy required for mixing (ERM; Shenoi et al. (2002)) the upper 60 m water column clearly show that during the barrier layer erosion, ERM was less compared to when barrier layer was present (Fig. 5b). This large difference in ERM between the time period when barrier layer was present and when barrier layer eroded is a consequence of the stratification in the upper 60 m water column. Even though the wind stress was maximum on 10 July, the ERM was also higher ($\tilde{} 3 \times 10^3 Jm^{-2}$) compared to 7 July , 2016 ($\tilde{} 1 \times 10^3 Jm^{-2}$). Hence, the deepening of MLD was inconsistent with the wind stress changes.

During the night, the net surface heat flux derived from the AWS was negative (Fig. 5a), indicating surface cooling and a negative buoyancy flux that was favorable for convection (Fig. 5b). Hence, this night-time negative buoyancy flux could potentially enhance mixing, leading to the erosion of the barrier layer. However, the negative buoyancy flux did not show any increase in magnitude during the barrier layer erosion period, as would be expected if this were the primary mechanism. Hence, wind and buoyancy flux do not appear to be the primary reasons for the barrier layer erosion. Throughout the time series, isothermal layer depth was approximately 60 m and barrier layer thickness was approximately 30 m except during the barrier layer erosion (Fig. 5c).

f. Salinity budget

As a step to understand the barrier layer formation and erosion in the southern BoB, salinity budget of upper 60 m, which included both the mixed layer and barrier layer is investigated. Tendency term showed positive values on 6–7 July and 12 July 2016 indi-

14

cating gain in salinity in the upper 60 m water column (Fig. 6a). Except for these days, tendency suggested negative values indicating loss of salinity. The advection term constructed using the western and southern uCTD sections indicate that major contribution to the tendency is the advection term (Fig. 6a). Advection term of the salinity budget is mostly contributed by the zonal advection except on 4–5 July and 12–13 July when vertical advection term had significant contribution to the tendency (Fig. 6b). This role of vertical advection term can be seen as the heaving of isotherms and isohalines at the base of barrier layer (Fig. 2a,b).

During the barrier layer erosion, the tendency of salinity was completely contributed by the advection term and of which major contributor was zonal advection. Since there were no rain events during the time series observation, major contributor for the surface flux was the evaporation (Fig. 6c). The daily averaged diapycnal salt flux between 60 to 80 m depth slab was more during the BL erosion (Fig. 6d). However, it can be seen that, surface salinity flux from evaporation and diapycnal salinity flux to the upper 60 m slab is 3 order lower than what contributed by the advection terms. Residual term includes all errors due to sampling and instrumentation. It has to be noted that both tidal and inertial period are not fully resolved in the calculation of horizontal and vertical gradients, respectively.

4. BL formation and suppression of turbulence

The barrier layer at the time series location was 30–40 m thick and observed during the freshening events (4–5 July and 10–14 July, 2016; Fig. 2a, b). CTD observations (not shown here) carried out 2 hour prior to the first microstructure profiler observation at the time series location showed a deeper MLD and relatively saline upper layer. There

15

was a decrease of 0.3 PSU in surface salinity from 34.3 to 33.9 PSU in 2 hour on 4 July, 2016 (Vinayachandran et al. 2018). Initial microstructure profiler observations at the time series location were during the phase of BL formation. In this section, we discuss barrier layer formation and how the wind effect is suppressed in the barrier layer.

a. Role of surface freshening

The barrier layer forms when the MLD becomes shallower than the isothermal layer due to the salinity stratification in the upper layer (Lukas and Lindstrom 1991; Vinay-achandran et al. 2002; Thadathil et al. 2007). To illustrate the effect of temperature and salinity on stratification, three night-time observations are presented: 1) barrier layer event 1, at the beginning of the time series when the surface salinity was 33.8 PSU (4 July 10:28 PM local time, blue lines in Fig. 7); 2) barrier layer erosion when the surface salinity was 34.3 PSU (07 July 10:53 PM local time, black); 3) barrier layer event 2 near the end of the time series (13 Jul 10:50 PM local time, red) when the surface layer freshened to 33.5 PSU (Fig. 7). The profiles (Fig. 7a) of temperature (dashed line) and salinity (continuous) during the freshening events clearly show that the MLD (shown by the coloured stars) was at the base of a freshened surface layer and the depth of the isothermal layer was approximately constant at 60 m.

In the selected profiles on 4, 7, and 13 July, values of salinity stratification ($N_S^2 = g\beta\frac{\partial S}{\partial z}$, Fig. 7b) at the MLD were respectively 1.5×10^{-4}, 3.8×10^{-4} and 6.0×10^{-4} s^{-1}, and thermal stratification ($N_T^2 = g\alpha\frac{\partial T}{\partial z}$, Fig. 7c) were 8.1×10^{-5}, 5.5×10^{-4} and 1.0×10^{-4} s^{-1} respectively. It can be seen that when the surface layer was characterized by low salinity waters, the contribution of salinity stratification was stronger than that by thermal stratification (red and blue profiles in Fig. 7b, c), at the MLD. However, during

16

the barrier layer erosion when the surface salinity was higher (34.5 PSU), thermal and salinity stratification were comparable (black profile in Fig. 7 b, c). These observations clearly suggest that the MLD was set at the base of the freshened surface layer in the two barrier layer events, and the barrier layer formed owing to the dominance of salinity stratification in the upper layer.

The time series location is characterized climatologically by a low salinity surface layer, typically advected from the north or northeastern BoB (Girishkumar et al. 2011; Thangaprakash et al. 2016; Girishkumar et al. 2017). The northern and northeastern BoB has its highest precipitation and runoff during the summer monsoon (Han et al. 2001; Wilson and Riser 2016; Mahadevan et al. 2016). Behara and Vinayachandran (2016), using an ocean general circulation model, showed that freshening in the eastern BoB is mainly contributed by the rainfall with a peak during the summer monsoon, and freshwater transport in the upper layer is generally southward. Satellite derived sea surface salinity suggests that the time series location was surrounded by low salinity water (Fig. 1). Since there was no spell of rain during the time series, it is likely that the freshening events were a result of advection. This is further supported by the salinity budget, where salinity tendency is mainly contributed by the advection terms (Fig. 6a, b).

b. Role of high salinity core

One of the mechanisms that maintains the thickness of the barrier layer is the preservation of the isothermal layer (Katsura et al. 2015). A heat budget analysis based on RAMA data at the time series location suggested that penetrative radiation through the thin mixed layer maintains the isothermal layer temperature (Girishkumar et al. 2011;

Thangaprakash et al. 2016; Girishkumar et al. 2017). In contrast, eddy diffusion of temperature at the base of the isothermal layer cools and enhances its erosion. However, during the BoBBLE experiment, the presence of high stratification at the base of the isothermal layer suppresses this eddy diffusion, reducing the cooling of the isothermal layer (Fig. 4b).

During most of the time series, at the base of the isothermal layer, stratification dominated over shear ($Ri > 0.25$) suppressing the shear-induced mixing (Fig. 3b). This stratification maximum at the base of the isothermal layer is associated with the presence of the subsurface high salinity core (Fig. 2b). This stratification maximum is stronger than that at the base of the mixed layer (Fig. 2d). While the stratification maximum at the base of the mixed layer was caused by salinity stratification, the maximum at the base of the isothermal layer was contributed more or less equally by haline and thermal stratification (Fig. 6b, c). The subsurface high salinity core is the manifestation of ASHSW transported by the subsurface branch of SMC (Vinayachandran et al. 2013; Jain et al. 2017; Vinayachandran et al. 2018; Webber et al. 2018). Thus, the stratification necessary for the formation and maintenance of the barrier layer in the southern BOB is facilitated by the surface freshened layer and the subsurface high salinity core.

c. Decay of turbulence in the barrier layer

TKE dissipation rates (ε) are large within the mixed layer (Fig. 4a), as expected. However, they are very low (close to the background value of 10^{-9} W kg^{-1}) within the barrier layer, even though it is a relatively homogeneous layer. The Richardson number is above the critical value (Ri > 0.25) within the barrier layer (Fig. 3b). Hence, even though the density stratification is relatively low, wind-induced shear within the barrier layer was

18

weak compared to the density stratification. This indicates a lack of Kelvin-Helmholtz instability (Lozovatsky et al. 2006), and therefore explains the weak turbulence in the barrier layer. However, exceptions were noted on 5, 10 and 13 July when $Ri < 0.25$ in the barrier layer and ε values were high. This was most probably due to internal wave breaking (Gargett and Holloway 1984). Except on these days, the barrier layer was characterized with weak ε.

In terms of the suppression of turbulence, the barrier layer at the time series location was comparable to that of the northern BoB, where the influence of river runoff and rainfall is more intense. Observations of mixing in the northern BoB (Lucas et al. 2016; Jinadasa et al. 2016) showed weak turbulence below the MLD due to the presence of the barrier layer. Vinayachandran et al. (2002), in their observations in the northern BOB during the summer monsoon, showed that following the arrival of freshwater plume, the surface salinity reduced significantly (up to 4 PSU), the MLD decreased and a barrier layer was formed. Rao et al. (2011) and Sengupta et al. (2016) also showed a similar decrease of surface salinity and formation of a barrier layer.

In contrast, at the BoBBLE time series location, the surface salinity decreased by 0.5 PSU and the barrier layer formed. The stratification required for the barrier layer was provided by both the low salinity surface layer and the high salinity core beneath the isothermal layer. This is unlike the northern BoB where the subsurface salinity maximum is at a depth greater than 250 m (Vinayachandran et al. 2013; Jain et al. 2017), and hence has less influence on the barrier layer.

5. BL erosion

At the BoBBLE time series location, erosion of the barrier layer was observed from 6–9 July, accompanied by an increase in surface salinity and deepening of the mixed layer (Fig. 2 b). During the barrier layer erosion, large values of mixing parameters (ε and K_ρ) penetrated down to 60 m (Fig. 4a, b). In this section, processes responsible for the erosion of the barrier layer and penetration of mixing are discussed in detail.

a. Role of horizontal advection

ADCP surface currents during the erosion of the barrier layer indicated weak eastward (˜0.2 m s^{-1}) currents (Fig. 3a). The close proximity of the SMC to the time series location (which is east of the SMC core; Fig. 1) suggests the possibility of advection of high salinity water from the Arabian Sea to the study region. Vinayachandran et al. (2013) and Mahadevan et al. (2016) showed that as the SMC brings high salinity water from the Arabian Sea, it gets fresher due to interaction with low salinity water from the northern BoB. The westward and southward uCTD sections from the time series location (Fig. 1 inset), carried out every evening, observed increased surface salinity during the barrier layer erosion (Fig. 8a, b). The slope of the high salinity patch (34.5 PSU) along the westward section (Fig. 8a) indicates eastward advection of high salinity water to the time series location. ADCP surface currents along the western uCTD section on 6 July was also eastward (Fig. 8a). This salinity patch was not captured by the SMAP salinity, probably due to the limited spatial (25 km) and temporal (weekly) resolution of the SMAP data set. The size of the high salinity patch can be estimated to be in the range of 25 km^2 to 10 km^2 as the uCTD section was approximately 10 km in length.

20

During the time series when the barrier layer was prominent, the upper ocean can be considered to be made up of three distinct homogeneous (in terms of salinity) layers of water in relative motion. From the surface downwards these are: a mixed layer ($<$33.8 PSU); a barrier layer with medium salinity (~34.4 PSU); a high salinity core ($>$35 PSU; Fig. 2b). At the interface of these layers, strong shear and stratification were present (Figs. 2d, 3b). Western uCTD sections from 5–7 July, 2016 (Fig. 8c,d,e) indicate that during the BL erosion the three layer structure of upper ocean was replaced with a deep mixed layer. This is consistent with the salinity budget analysis of upper 60 m. Salinity budget of upper 60 m water column clearly suggested that daily tendency of salinity was positive on 6–7 July and started decreasing till 9–10 July, 2016. The tendency during this period was contributed by advective terms especially the zonal advection term (Fig. 6a, b) and the residue was at its minimum. During 6–7 July the upper 60 m current was generally eastward or southeastward (Fig. 3a). Therefore, together with the slope of high sea surface salinity core in the westward time-longitude uCTD section and salinity budget analysis, it is confirmed that the salinisation event was due to the advection of high salinity water from the SMC.

The replacement of three layer stratified structure of upper ocean with a deep mixed layer during barrier layer erosion, further allowed the surface forcing to penetrate to a deeper depth. This was evident in the elevated ε ($> 10^{-7}$ W kg^{-1}, Fig. 4a) and K_ρ ($> 10^{-4}$ m s^{-2}, Fig. 4b) penetrated down to 60 m. Thus the advection of the high surface salinity patch to the time series location reduced the vertical stratification, and the surface forcing penetrated to greater depths

21

b. Role of vertical shear

Shear layers will promote mixing and can lead to the erosion of the barrier layer. ADCP data collected during the time series observation highlights the presence of two shear maxima, one at the base of the mixed layer and the other at the base of the barrier layer (Fig. 3b). The high shear layer noted at the base of the mixed layer was due to the wind work (Fig. 5c, Moum and Smyth (2001)). Near inertial oscillations can also generate enhanced shear at the base of mixed layer (Johnston et al. 2016). Since the inertial period of the study region is 3.6 days, 10 days time series could not fully resolve the near inertial oscillations. The relative motion of the barrier layer (weak currents) and the high salinity core (strong southward currents) caused the shear maximum at the base of the barrier layer (Fig. 3a). The presence of two shear maxima in the upper ocean was observed throughout the cruise from the core of SMC (85°E) to 89°E along 8°N. This feature was also observed during the western and southern uCTD sections. At the beginning of the salinisation event (5–6 July), when the stratification at the interface between the mixed layer and barrier layer weakened (Fig. 2d), the vertical shear strengthened (Fig. 3b), which induced vertical mixing (Fig. 4a,b).

In addition, the high shear layer at the interface of the barrier layer and the high salinity core can also cause shear instability and vertical mixing, indicated by patches of $Ri < 0.25$ at the base of the mixed layer and barrier layer (Fig. 3b). Note that, owing to the two high shear layers at the top and the base of the barrier layer, even a slight reduction in stratification can cause shear instability and trigger mixing (Lozovatsky et al. 2006), resulting in barrier layer erosion. When the barrier layer eroded, the background stratification within the deeper mixed layer decreased, due to the increase in surface

salinity (appearance of high salinity patch from the SMC). Except during the salinisa-tion event, the two-layer shear maxima structure was unable to break the barrier layer, since the high salinity patch (34.35 PSU) was replaced by a low salinity layer (33.8 PSU) and the surface stratification was strengthened.

This double shear layer structure observed here in the southern BoB is in contrast to the shear layer structure of barrier layers in the northern BoB. Recent micro-structure observations in the northern BoB by Lucas et al. (2016) showed suppressed mixing, and a relatively stronger barrier layer attributed to the fresher surface layer, with an absence of strong shear at the base of the barrier layer. They concluded that the lack of strong shear at the base of the barrier layer might be the reason for the low subsurface mixing rate observed in the northern BoB. Our observations in the southern BoB showed a comparable barrier layer with a relatively less freshened surface layer (compared to the northern BoB), a salinity maximum at the base of the barrier layer and the presence of high shear layers both at the top and the bottom of the barrier layer (Fig. 3c). Thus, the presence of two shear maxima, one above and the other below the barrier layer makes the southern BoB barrier layer vulnerable to erosion.

c. Role of vertical mixing

Vertical mixing tends to homogenize the vertical gradient and reduce the stratification. Since the barrier layer is mainly controlled by the haline stratification, the focus here is on the vertical mixing of salt. When the barrier layer was prominent, the time-depth section of the vertical salinity gradient showed two maxima, one at the base of the mixed layer and the other at the base of barrier layer (Fig. 4c). During the barrier layer erosion, elevated mixing penetrated deeper (Fig. 4a, b) and reduced the vertical salinity gradient

23

in the upper 60 m. As discussed in the previous sections, major sources of vertical mixing were surface forcing (wind and buoyancy), shear instability and internal wave breaking. In general, K_ρ was less than 10^{-5} $m^2 s^{-1}$ during the time series, indicating weak turbulent vertical mixing at the base of the mixed layer (Fig. 4 b). Exceptions were noticed on 4, 5, 10 and 11 July where K_ρ was greater than 10^{-4} $m^2 s^{-1}$. On these days surges of upward salt flux $J_s > 1$ mg m^{-2} s^{-1} were noticed at the base of the mixed layer (Fig. 4d). Most of these surges were associated with the shear layer maximum (Fig. 3d) where $Ri < 0.25$. However, surface salinity changes observed during the time series cannot be accounted for by these surges in the diapycnal salt flux.

To understand the salinity contribution by the diapycnal flux of salt from the high salinity core to the upper 60 m, turbulent flux term is calculated as the product of $< K_\rho >$ and the vertical salinity gradient in the 60–80 m layer (Fig. 6d). Turbulent flux term showed elevated values during the barrier layer erosion, but contributed very less to the salinity tendency of upper 60 m (Fig. 6a). This suggests that advective processes were dominant during both the salinisation and freshening events.

6. Modeling

An ocean model was employed to understand the role of background stratification on the TKE dissipation rate ε during the period of observation. The model was the one-dimensional General Ocean Turbulence Model (GOTM, Umlauf and Burchard (2005)) implementation of the two equation K-ε scheme (Canuto et al. 2001) with dynamic dissipation rate equations for the length scales. Using the same model, Stips et al. (2002) simulated observed ε reasonably well. The time step for the model run was 1 hour. The depth of the column was 250 m with a 1 m vertical grid spacing. Details of the model

24

setup are given in Table 1. The model was forced with heat and momentum fluxes calculated using the AWS data. Four experimental runs were carried out to examine the processes leading to the observed ε:

(1) No Relax; the model was forced with wind and atmospheric fluxes, and initiated with the first temperature and salinity profiles of the observed time series (Fig. 8a).

(2) Full Relax; forced with wind and atmospheric fluxes, but model temperature and salinity relaxed to the observed temperature and salinity (Fig. 8b).

(3) Only Flux; forced with only the atmospheric heat fluxes, but model temperature and salinity were relaxed to the observed temperature and salinity (Fig. 8c).

(4) Only Wind; forced only with the wind, but model temperature and salinity were relaxed to the observed temperature and salinity (Fig. 8d).

Because of the lack of advection in the one-dimensional model, the No Relax run does not contain the barrier layer erosion and reformation events that were observed in the BoBBLE time series. However, the Full Relax run does contain a representation of the barrier layer erosion and reformation events, as the model temperature and salinity were relaxed to observations throughout the model run.

In the No Relax run (Fig. 8a), the maximum downward penetration of elevated ε values occurred on 10 July when the wind was at its peak. In contrast, in the observations the maximum penetration of elevated ε values occurred on 7 July (Fig. 4a). When the model was relaxed to the observed temperature and salinity (Full Relax run, Fig. 8b), the ε model behavior followed the observed behavior closely. Hence, the realistic stratification in the Full Relax run (originating from the relaxation to observed temperature and salinity fields throughout the run) are a key component in the successful simulation of the correct mixing fields.

25

The Full Relax run also captured the low turbulence in the barrier layer and a patchy elevated ε at the base of the barrier layer. The upper layer ε, however, was an order of magnitude lower than that of the observed, probably because Langmuir turbulence and wave breaking turbulence were not represented in the model physics. From the runs with 'Only Flux' (Fig. 8c) and 'Only Wind' (Fig. 8d), it was clear that even though the negative buoyancy flux due to the night-time cooling aided the turbulence, the major contributor was the wind forcing.

The above GOTM experiments suggest that, in the southern BoB, to simulate the observed mixing rates in the upper ocean, the model had to reproduce the stratification close to the observations, which was mainly dictated by the advective processes. The observed diapycnal flux (Fig. 4d) and the diapycnal flux calculated using the eddy diffusivity of salt from the Full Relax GOTM run (Fig. 9b) compared well below the surface layer (where wave breaking and Langmuir turbulence dominated). The deep penetration of enhanced diapycnal salt flux noticed during the barrier layer erosion, and the weak flux within the barrier layer, were captured by the Full Relax GOTM run. However, the diapycnal salt flux calculated using the eddy diffusivity of salt from the No Relax run could not capture the deep penetration of elevated diapycnal slat flux observed during the barrier layer erosion (Fig. 9a). This further indicates the need for ocean models to capture the stratification accurately in order to simulate the turbulence field realistically.

7. Summary and conclusion

The 10-day time series of micro-structure observations carried out at 8ºN, 89ºE in the southern BoB during the summer monsoon of 2016 as a part of the BoBBLE field campaign captured a barrier layer erosion and reformation event. During the barrier

26

layer erosion, the mixed layer deepened from 20 m to 60 m, and the TKE dissipation rate (ε) and eddy diffusivity (K_ρ) showed elevated values of $> 10^{-7}$ W kg^{-1} and $> 10^{-4}$ m^2 s^{-1} respectively, in the upper 60 m, and surface salinity increased from 33.84 to 34.35 PSU. After the barrier layer erosion, the surface salinity decreased to 33.8 PSU, the mixed layer shallowed to 20 m, the barrier layer re-formed and elevated mixing rates were confined to the upper 20 m.

The observed barrier layer was 30–40 m thick and formed due to low salinity waters (33.35 to 33.8 PSU) advected to the time series location. The salinity induced stratification confined the MLD to the base of the relatively freshened surface layer of ˜20 m thickness while the isothermal layer extended to ˜60 m. The presence of a stratification maximum just beneath the isothermal layer suppressed cooling from below by eddy diffusion and the temperature of the isothermal layer was thus maintained. The stratification maxima below the isothermal layer was co-located with the subsurface high salinity core, a manifestation of the subsurface intrusion of ASHSW via the SMC. The low salinity surface layer and high salinity subsurface layer at the base of isothermal layer together provided the stratification necessary for the maintenance of the barrier layer at the time series location.

ε and K_ρ profiles derived from micro-structure shear measurements suggest that, when the barrier layer was prominent, the influence of surface forcing was confined to the mixed layer and the barrier layer was characterized by suppressed turbulent mixing. The strong stratification within the barrier layer dampened the effect of surface wind on the turbulence below the mixed layer.

There are marked differences in the formation of the barrier layer between the southern and northern BoB. The low salinity surface layer of the southern BoB is less fresh

27

compared to that of the northern BoB. The stratification necessary for the formation and maintenance of the barrier layer in the southern BoB is provided by both the freshened surface layer and the subsurface high salinity intrusion associated with the SMC. In the northern BoB, below the MLD, waters are continuously stratified and the subsurface high salinity maxima observed is much deeper than the isothermal layer base, hence having less impact on the isothermal layer of the northern BoB (Vinayachandran et al. 2013; Jain et al. 2017). The observation of shear maxima, at the top and bottom of the barrier layer in the southern BoB during the time series reported here was also different from that observed in the northern BoB (Lucas et al. 2016), where elevated shear was present only at the mixed layer base. These two layers of shear maxima are important since any reduction in stratification can result in shear instability, and in turn trigger vertical mixing making the barrier layer in the southern BoB more prone to erosion.

There was an increase in sea surface salinity of 0.5 PSU (salinisation event) during the barrier layer erosion period. ADCP currents, uCTD time-longitude surface salinity sections, and salinity budget of upper 60 m water column revealed that advection of a high salinity and deep mixed layer patch from the SMC to the time series location was the cause of this salinisation event. During the salinisation event, the background stratification weakened and the surface forcing penetrated to a deeper layer. The weakening of stratification also resulted in shear induced mixing, and contributed to the increase of ε ($> 10^{-7}$ W kg^{-1}) and K_ρ ($> 10^{-3}$ m^2 s^{-1}) down to 60 m.

The weak turbulent flux term of the salinity budget (3 order lower than the tendency term) at the high salinity core (60–80m depth) clearly suggests that vertical mixing did not contribute significantly to the observed salinisation event. The weak upward diapyc-

nal flux of salt from the high salinity core was mainly because of the strong stratification at the top of the high salinity core, and weak winds during the barrier layer erosion.

Our analysis suggests a close link between ocean dynamics and air–sea interaction. A high salinity patch with weak background stratification transported by the SMC to a freshened and stratified BoB is a potential spot for reduced air-sea interaction, as the destruction of the barrier layer increases the mixed layer depth, reducing the sensitivity of the mixed layer temperature (and SST) to atmospheric surface fluxes. The subsequent advection of a surface fresh layer and reformation of the barrier layer decreased the mixed layer depth, enhancing potential air–sea interaction.

APPENDIX

Estimation of salinity budget terms

The tendency of salinity in the upper 60 m were computed by first evaluating $\frac{\partial S}{\partial t}$ as a function of depth and then integrating vertically from 60 m depth to the surface. $\frac{\partial S}{\partial t}$ were

29

estimated by fitting a straight line through time series of VMP salinity data each day at each depth following Feng et al. (1998). The slope of the least square fit was taken as the daily-mean time derivative for a given depth. The spatial gradients of salinity $\frac{\partial S}{\partial x}$ and $\frac{\partial S}{\partial y}$ was calculated from the daily westward and southward uCTD sections by a least square fitting at each depth respectively. Horizontal velocity components were obtained from daily averaged ship-mounted ADCP measurements at the time series location. uCTD produced daily one and total 10 zonal depth (x-z) and meridional depth (y-z) sections. The length and depth of each transect was 10 km and 200 m, respectively. Individual (x-z) and (y-z) sections were separated by approximately 4 hours.

To calculate the vertical velocity using the conservation of mass, vertical gradient of density was calculated from 1 m center difference of the daily averaged density profiles at time series location. The spatial gradients of density were calculated from the uCTD sections by linear fitting similar to salinity. Surface flux term was calculated using daily mean evaporation and surface salinity. Turbulent flux of salinity to upper 60 m water column is calculated as the daily averaged diapycnal salt flux between 60 to 80 m depth slab.

References

Akhil, V., and Coauthors, 2014: A modeling study of the processes of surface salinity seasonal cycle in the Bay of Bengal. *J. Geophys. Res.: Oceans*, **119 (6)**, 3926–3947.

Balaguru, K., P. Chang, R. Saravanan, L. R. Leung, Z. Xu, M. Li, and J.-S. Hsieh, 2012: Ocean barrier layers effect on tropical cyclone intensification. *Proceedings of the National Academy of Sciences*, **109 (36)**, 14 343–14 347.

Behara, A., and P. Vinayachandran, 2016: An OGCM study of the impact of rain and river water forcing on the Bay of Bengal. *J. Geophys. Res.: Oceans*, **121 (4)**, 2425–2446.

Callaghan, A. H., B. Ward, and J. Vialard, 2014: Influence of surface forcing on near-surface and mixing layer turbulence in the tropical Indian Ocean. *Deep Sea Res., Part I*, **94**, 107–123.

Canuto, V. M., A. Howard, Y. Cheng, and M. Dubovikov, 2001: Ocean turbulence. Part I: One-point closure model-Momentum and heat vertical diffusivities. *J. Phys. Oceanogr.*, **31 (6)**, 1413–1426.

Cheng, Y., V. Canuto, and A. Howard, 2002: An improved model for the turbulent PBL. *J. Atmos. Sci.*, **59 (9)**, 1550–1565.

Chowdary, J. S., A. Parekh, S. Ojha, and C. Gnanaseelan, 2015: Role of upper ocean processes in the seasonal SST evolution over tropical Indian Ocean in climate fore-casting system. *Climate Dyn.*, **45 (9-10)**, 2387–2405.

Das, U., P. Vinayachandran, and A. Behara, 2016: Formation of the southern Bay of Bengal cold pool. *Climate Dyn.*, **47 (5-6)**, 2009–2023.

de Boyer Montégut, C., J. Mignot, A. Lazar, and S. Cravatte, 2007: Control of salinity on the mixed layer depth in the world ocean: 1. General description. *J. Geophys. Res.: Oceans*, **112 (C6)**.

Drazin, P. G., and W. H. Reid, 2004: *Hydrodynamic stability*. Cambridge university press.

31

Drushka, K., W. E. Asher, B. Ward, and K. Walesby, 2016: Understanding the formation and evolution of rain-formed fresh lenses at the ocean surface. *J. Geophys. Res.: Oceans*, **121 (4)**, 2673–2689.

Durand, F., D. Shankar, C. de Boyer Montégut, S. Shenoi, B. Blanke, and G. Madec, 2007: Modeling the barrier-layer formation in the southeastern Arabian Sea. *J. Climate*, **20 (10)**, 2109–2120.

Entekhabi, D., and Coauthors, 2010: The soil moisture active passive (SMAP) mission. *Proc. IEEE*, **98 (5)**, 704–716.

Fairall, C., E. F. Bradley, J. Hare, A. Grachev, and J. Edson, 2003: Bulk parameterization of air–sea fluxes: Updates and verification for the COARE algorithm. *J. Climate*, **16 (4)**, 571–591.

Feng, M., P. Hacker, and R. Lukas, 1998: Upper ocean heat and salt balances in response to a westerly wind burst in the western equatorial pacific during toga coare. *Journal of Geophysical Research: Oceans*, **103 (C5)**, 10 289–10 311.

Gargett, A. E., and G. Holloway, 1984: Dissipation and diffusion by internal wave breaking. *J. Mar. Res.*, **42 (1)**, 15–27.

Girishkumar, M., M. Ravichandran, M. McPhaden, and R. Rao, 2011: Intraseasonal variability in barrier layer thickness in the south central Bay of Bengal. *J. Geophys. Res.: Oceans*, **116 (C3)**.

Girishkumar, M. S., J. Joseph, V. P. Thangaprakash, P. Vijay, and M. J. McPhaden, 2017: Mixed Layer Temperature Budget for the Northward Propagating Summer Monsoon

Intraseasonal Oscillation (MISO) in the Central Bay of Bengal. *J. Geophys. Res.: Oceans*, **122 (11)**, 8841–8854.

Gregg, M., E. D'Asaro, J. Riley, and E. Kunze, 2018: Mixing efficiency in the ocean. *Annual review of marine science*, **10**, 443–473.

Han, W., J. P. McCreary, and K. E. Kohler, 2001: Influence of precipitation minus evaporation and Bay of Bengal rivers on dynamics, thermodynamics, and mixed layer physics in the upper Indian Ocean. *J. Geophys. Res.: Oceans*, **106 (C4)**, 6895–6916.

Jain, V., and Coauthors, 2017: Evidence for the existence of Persian Gulf Water and Red Sea Water in the Bay of Bengal. *Climate Dyn.*, **48 (9-10)**, 3207–3226.

Jensen, T. G., 2003: Cross-equatorial pathways of salt and tracers from the northern Indian Ocean: Modelling results. *Deep Sea Res., Part II*, **50 (12)**, 2111–2127.

Jinadasa, S., I. Lozovatsky, J. Planella-Morató, J. D. Nash, J. A. MacKinnon, A. J. Lucas, H. W. Wijesekera, and H. J. Fernando, 2016: Ocean turbulence and mixing around Sri Lanka and in adjacent waters of the northern Bay of Bengal. *Oceanography*, **29 (2)**, 170–179.

Johnston, T. S., D. Chaudhuri, M. Mathur, D. L. Rudnick, D. Sengupta, H. L. Simmons, A. Tandon, and R. Venkatesan, 2016: Decay mechanisms of near-inertial mixed layer oscillations in the bay of bengal. *Oceanography*, **29 (2)**, 180–191.

Kara, A. B., P. A. Rochford, and H. E. Hurlbut, 2000: Mixed layer depth variability and barrier layer formation over the North Pacific Ocean. *J. Geophys. Res.: Oceans*, **105 (C7)**, 16 783–16 801.

33

Katsura, S., E. Oka, and K. Sato, 2015: Formation Mechanism of Barrier Layer in the Subtropical Pacific. *J. Phys. Oceanogr.*, **45 (11)**, 2790–2805.

Lagerloef, G., G. Mitchum, F. Bonjean, and R. Cheney, 2002: OSCAR (Ocean Surface Currents Analysis-Real time): An Operational Resource for Various Maritime Applications and El Niño Monitoring in the Tropical Pacific Using Jason-1 Data. *AGU Fall Meeting Abstracts*.

Lee, J.-Y., B. Wang, M. C. Wheeler, X. Fu, D. E. Waliser, and I.-S. Kang, 2013: Real-time multivariate indices for the boreal summer intraseasonal oscillation over the asian summer monsoon region. *Climate Dynamics*, **40 (1-2)**, 493–509.

Li, Y., W. Han, M. Ravichandran, W. Wang, T. Shinoda, and T. Lee, 2017: Bay of Bengal salinity stratification and Indian summer monsoon intraseasonal oscillation: 1. Intraseasonal variability and causes. *J. Geophys. Res.: Oceans*, **122 (5)**, 4291–4311.

Lozovatsky, I., E. Roget, H. Fernando, M. Figueroa, and S. Shapovalov, 2006: Sheared turbulence in a weakly stratified upper ocean. *Deep Sea Res., Part I*, **53 (2)**, 387–407.

Lucas, A. J., and Coauthors, 2016: Adrift upon a salinity-stratified sea: a view of upper-ocean processes in the Bay of Bengal during the southwest monsoon. *Oceanography*, **29 (2)**, 134–145.

Lukas, R., and E. Lindstrom, 1991: The mixed layer of the western equatorial Pacific Ocean. *J. Geophys. Res.: Oceans*, **96 (S01)**, 3343–3357.

MacKinnon, J. A., and Coauthors, 2016: A tale of two spicy seas. *Oceanography*, **29 (2)**, 50–61.

Maes, C., and T. J. O'Kane, 2014: Seasonal variations of the upper ocean salinity stratification in the Tropics. *J. Geophys. Res.: Oceans*, **119 (3)**, 1706–1722.

Mahadevan, A., G. S. Jaeger, M. Freilich, M. M. Omand, E. L. Shroyer, and D. Sengupta, 2016: Freshwater in the Bay of Bengal: Its fate and role in air-sea heat exchange. *Oceanography*, **29 (2)**, 72–81.

Matthews, A. J., and Coauthors, 2015: BoBBLE: Bay of Bengal Boundary Layer Experiment. *CLI-VAR Exchanges*, **19 (68)**, 38–41.

Mellor, G. L., 1989: Retrospect on oceanic boundary layer modeling and second moment closure. *Parameterization of Small-scale Processes. Proceedings of the Aha Hulikoa Hawaiian Winter Workshop, Honolulu, University of Hawaii at Manoa*, 251–271.

Mignot, J., C. de Boyer Montégut, A. Lazar, and S. Cravatte, 2007: Control of salinity on the mixed layer depth in the world ocean: 2. Tropical areas. *J. Geophys. Res.: Oceans*, **112 (C10)**.

Moum, J., and W. Smyth, 2001: Upper ocean mixing processes. *Encyclopedia of Ocean Sciences*, **6**, 3093–3100.

Moum, J. N., D. R. Caldwell, and C. A. Paulson, 1989: Mixing in the equatorial surface layer and thermocline. *J. Geophys. Res.: Oceans*, **94 (C2)**, 2005–2022.

Murty, V., Y. Sarma, D. Rao, and C. Murty, 1992: Water characteristics, mixing and circulation in the Bay of Bengal during southwest monsoon. *J. Mar. Res.*, **50 (2)**, 207–228.

Osborn, T., 1980: Estimates of the local rate of vertical diffusion from dissipation measurements. *J. Phys. Oceanogr.*, **10 (1)**, 83–89.

Rao, R., and R. Sivakumar, 2003: Seasonal variability of sea surface salinity and salt budget of the mixed layer of the north Indian Ocean. *J. Geophys. Res.: Oceans*, **108 (C1)**.

Rao, S. A., and Coauthors, 2011: Modulation of SST, SSS over northern Bay of Bengal on ISO time scale. *J. Geophys. Res.: Oceans*, **116 (C9)**.

Rodi, W., 1987: Examples of calculation methods for flow and mixing in stratified fluids. *J. Geophys. Res.: Oceans*, **92 (C5)**, 5305–5328.

Roget, E., I. Lozovatsky, X. Sanchez, and M. Figueroa, 2006: Microstructure measurements in natural waters: Methodology and applications. *Prog. Oceanogr.*, **70 (2)**, 126–148.

Sengupta, D., G. Bharath Raj, M. Ravichandran, J. Sree Lekha, and F. Papa, 2016: Near-surface salinity and stratification in the north Bay of Bengal from moored observations. *Geophys. Res. Lett.*, **43 (9)**, 4448–4456.

Sengupta, D., and M. Ravichandran, 2001: Oscillations of bay of bengal sea surface temperature during the 1998 summer monsoon. *Geophysical Research Letters*, **28 (10)**, 2033–2036.

Shenoi, S., D. Shankar, and S. Shetye, 2002: Differences in heat budgets of the near-surface Arabian Sea and Bay of Bengal: Implications for the summer monsoon. *J. Geophys. Res.: Oceans*, **107 (C6)**.

Shetye, S., A. Gouveia, D. Shankar, S. Shenoi, P. Vinayachandran, D. Sundar, G. Michael, and G. Nampoothiri, 1996: Hydrography and circulation in the western Bay of Bengal during the northeast monsoon. *J. Geophys. Res.: Oceans*, **101 (C6)**, 14 011–14 025.

Shetye, S., S. Shenoi, A. Gouveia, G. Michael, D. Sundar, and G. Nampoothiri, 1991: Wind-driven coastal upwelling along the western boundary of the Bay of Bengal during the southwest monsoon. *Cont. Shelf Res.*, **11 (11)**, 1397–1408.

Smyth, W., P. Zavialov, and J. Moum, 1997: Decay of turbulence in the upper ocean following sudden isolation from surface forcing. *J. Phys. Oceanogr.*, **27 (5)**, 810–822.

Sprintall, J., and M. Tomczak, 1992: Evidence of the barrier layer in the surface layer of the tropics. *J. Geophys. Res.: Oceans*, **97 (C5)**, 7305–7316.

Stips, A., H. Burchard, K. Bolding, and W. Eifler, 2002: Modelling of convective turbulence with a two-equation k- turbulence closure scheme. *Ocean Dyn.*, **52 (4)**, 153–168.

Thadathil, P., S. I., G. S., P. K. S., L. Matthieu, R. R. R., N. S., and H. Akshay, 2016: Surface layer temperature inversion in the Bay of Bengal: Main characteristics and related mechanisms. *Journal of Geophysical Research: Oceans*, **121 (8)**, 5682–5696, doi:10.1002/2016JC011674, URL https://agupubs.onlinelibrary.wiley.com/doi/abs/10.1002/2016JC011674, https://agupubs.onlinelibrary.wiley.com/doi/pdf/10.1002/2016JC011674.

Thadathil, P., P. Muraleedharan, R. Rao, Y. Somayajulu, G. Reddy, and C. Revichandran, 2007: Observed seasonal variability of barrier layer in the Bay of Bengal. *J. Geophys. Res.: Oceans*, **112 (C2)**.

Thangaprakash, V., and Coauthors, 2016: What controls seasonal evolution of sea surface temperature in the Bay of Bengal? Mixed layer heat budget analysis using moored buoy observations along 90 E. *Oceanography*, **29 (2)**, 202–213.

Thorpe, S. A., 2007: *An introduction to ocean turbulence*. Cambridge University Press.

Ullman, D. S., and D. Hebert, 2014: Processing of Underway CTD data. *J. Atmos. Oceanic Technol.*, **31 (4)**, 984–998.

Umlauf, L., and H. Burchard, 2005: Second-order turbulence closure models for geophysical boundary layers. A review of recent work. *Cont. Shelf Res.*, **25 (7)**, 795–827.

Vidya, P., S. Das, and Coauthors, 2017: Contrasting Chl-a responses to the tropical cyclones Thane and Phailin in the Bay of Bengal. *J. Mar. Syst.*, **165**, 103–114.

Vinayachandran, P., Y. Masumoto, T. Mikawa, and T. Yamagata, 1999: Intrusion of the southwest monsoon current into the Bay of Bengal. *J. Geophys. Res.: Oceans*, **104 (C5)**, 11 077–11 085.

Vinayachandran, P., V. Murty, and V. Ramesh Babu, 2002: Observations of barrier layer formation in the Bay of Bengal during summer monsoon. *J. Geophys. Res.: Oceans*, **107 (C12)**.

Vinayachandran, P., D. Shankar, S. Vernekar, K. Sandeep, P. Amol, C. Neema, and A. Chatterjee, 2013: A summer monsoon pump to keep the Bay of Bengal salty. *Geophys. Res. Lett.*, **40 (9)**, 1777–1782.

Vinayachandran, P., and Coauthors, 2018: Bobble (bay of bengal boundary layer experiment): Ocean–atmosphere interaction and its impact on the south asian monsoon. *Bulletin of the American Meteorological Society*, **(2018)**.

Waterhouse, A. F., and Coauthors, 2014: Global patterns of diapycnal mixing from measurements of the turbulent dissipation rate. *J. Phys. Oceanogr.*, **44 (7)**, 1854–1872.

Webber, B. G. M., A. J. Matthews, P. N. Vinayachandran, C. P. Neema, A. Sanchez-Franks, V. Vijith, P. Amol, and D. B. Baranowski, 2018: The dynamics of the southwest monsoon current in 2016 from high-resolution in situ observations and models. *Journal of Physical Oceanography*, **0 (0)**, null, doi:10.1175/JPO-D-17-0215.1, URL https://doi.org/10.1175/JPO-D-17-0215.1, https://doi.org/10.1175/JPO-D-17-0215.1.

Wilson, E. A., and S. C. Riser, 2016: An assessment of the seasonal salinity budget for the upper Bay of Bengal. *J. Phys. Oceanogr.*, **46 (5)**, 1361–1376.

Yan, Y., L. Li, and C. Wang, 2017: The effects of oceanic barrier layer on the upper ocean response to tropical cyclones. *J. Geophys. Res.: Oceans*, **122 (6)**, 4829–4844.

You, Y., 1995: Salinity variability and its role in the barrier-layer formation during TOGA-COARE. *J. Phys. Oceanogr.*, **25 (11)**, 2778–2807.

LIST OF TABLES

TABLE 1. GOTM model setup.

| Turbulence Method	Second-Order Model
Type of second-order model	Explicit Algebraic Model with quasi equilibrium
Type of equation for buoyancy variance	Algebraic equation
Type of equation for variance destruction	Algebraic equation
Coefficients of second-order model	Cheng et al. (2002)
Dissipative length-scale method	Dynamic dissipation rate equation
TKE equation	dynamic equation (k-epsilon style)
TKE equation parameters	Rodi (1987)
Upper and lower boundary condition for k-equation	Flux boundary condition
Upper and lower boundary condition for length-scale equation	Flux boundary condition
Upper boundary layer	Logarithmic law of the wall
Lower boundary layer	Logarithmic law of the wall
Internal Wave Model	Mellor (1989)
Relaxation time	3600 s

FIG. 1. SMAP salinity overlaid by OSCAR current vectors, both averaged for the period of the time series observations (4–14 July, 2016). The red star represents the time series location (TSE,8°N 89°E) and the blue circles in the inset show the daily uCTD sections covered during the time series. Magenta arrows represent branches of the Summer Monsoon Current.

44
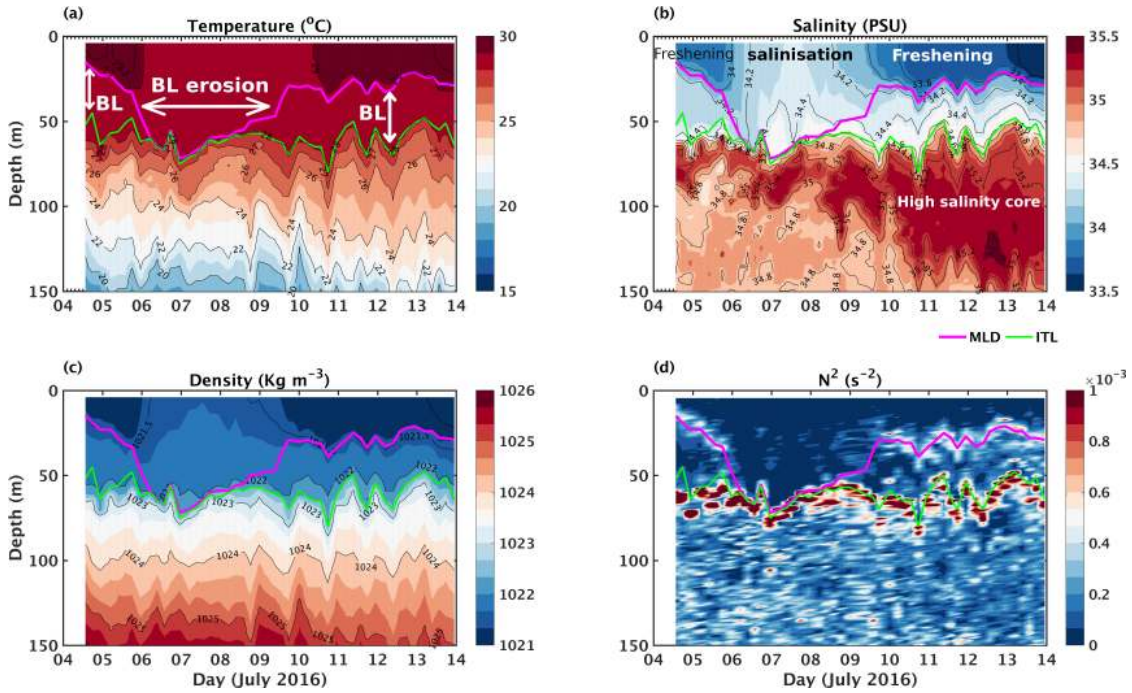
FIG. 2. Time–depth sections of hydrographic properties during the time series (4–14 July 2016) at 8°N 89°E: (a) temperature (°C), (b) salinity, (c) density (kg m^{-3}), (d) buoyancy frequency squared (N^2, s^{-2}). The magenta and green lines represent the MLD and isothermal layer depth, respectively.
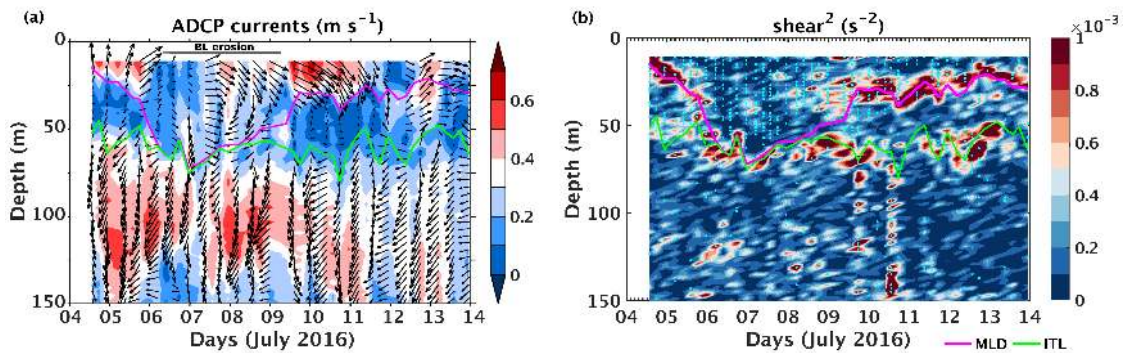
FIG. 3. Time–depth sections of (a) ADCP current speed (m s^{-1}) overlaid by the horizontal current vectors and (b) vertical shear (s^{-2}) during 4–14 July 2016 at the time series location. The cyan dots in panel (b) indicate the region where $Ri < 0.25$. The magenta and green lines represent the MLD and isothermal layer depth, respectively.
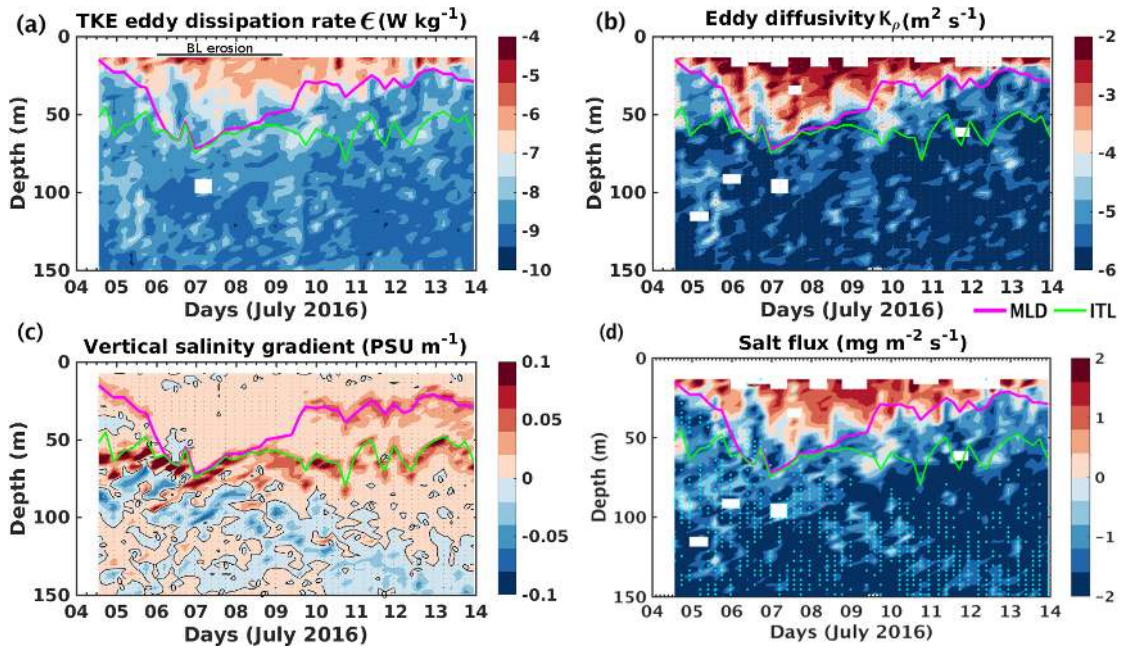
FIG. 4. Time–depth sections of: (a) $\log_{10}$ TKE dissipation rate ε (W kg^{-1}, (b) $\log_{10}$ eddy diffusivity K_ρ (m^2 s^{-1}), (c) vertical salinity gradient (PSU m^{-1}), (d) $\log_{10}$ of modulus of diapycnal salt flux (mg m^{-2} s^{-1}). The cyan dots in panel (d) indicate the regions where the salt flux is downward. The magenta and green lines represent the MLD and isothermal layer depth, respectively.
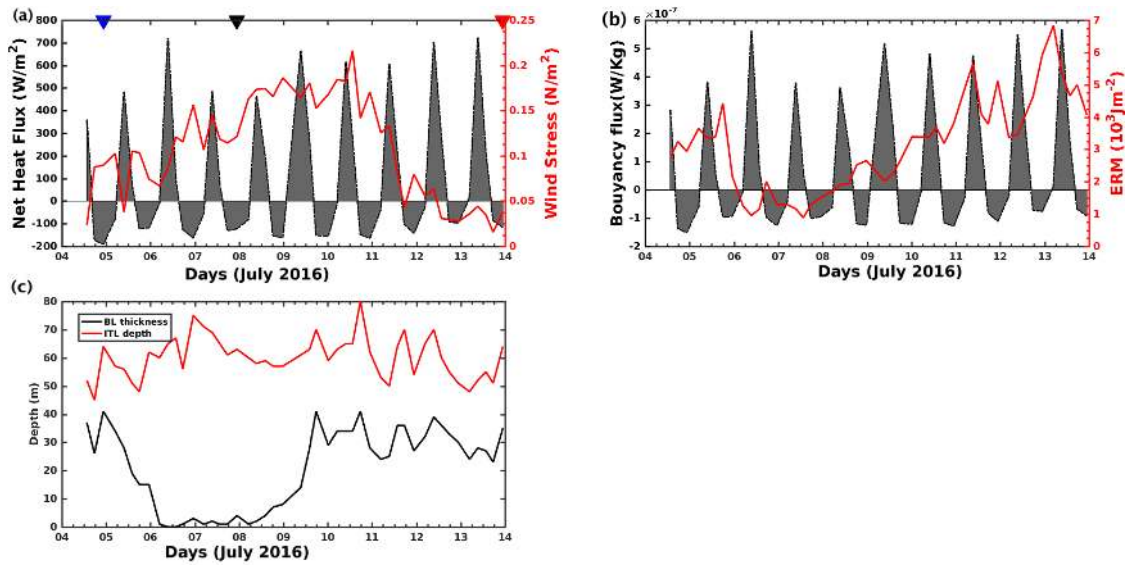
FIG. 5. (a) Time series of net heat flux (black; W m^{-2}) and wind stress (red; N m^{-2}). The triangles at the top of the panel represent the stations selected for detailed analysis (refer to Fig. 6) (b) Time series of buoyancy flux (black; W kg^{-1}), and energy required for mixing (ERM) the upper 60 m (red). (c)Time series of isothermal layer (ITL) depth (red) and barrier layer (BL) thickness (black).

48
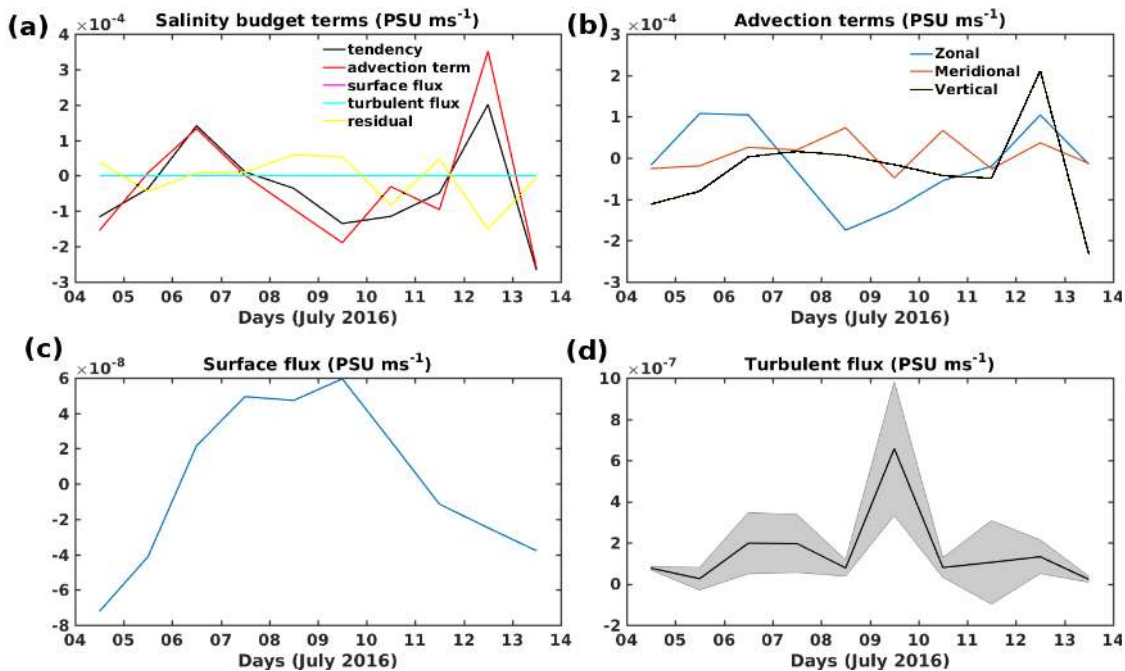
FIG. 6. (a)Time series of daily salinity budget terms; tendency (black), advection (red), surface flux (magenta), turbulent flux (cyan), residual (yellow)(b) Advection terms in the salinity budget; zonal (blue), meridional(red),vertical(black) (c)surface flux term (d) Turbulent flux term. Shaded region indicates the standard deviation.
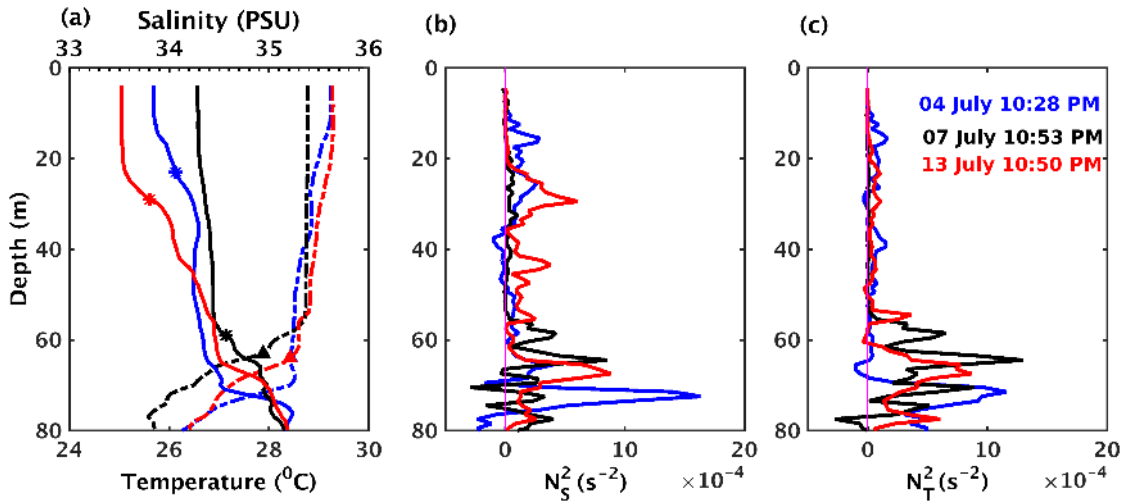
49

FIG. 7. Selected profiles of different properties during the time series observation for: 1) barrier layer event 1, 4 July 2016 10:28 PM, local time (blue); 2) barrier layer erosion, 7 July 2016 10:53 PM (black); 3) barrier layer event 2, 13 July 2016 10:50 PM (red). (a) Temperature (dashed line) and salinity (continuous line) profile. The filled triangle represents isothermal layer depth and the star represents MLD. (b) Salinity stratification (N_S^2). (c) Thermal stratification (N_T^2).
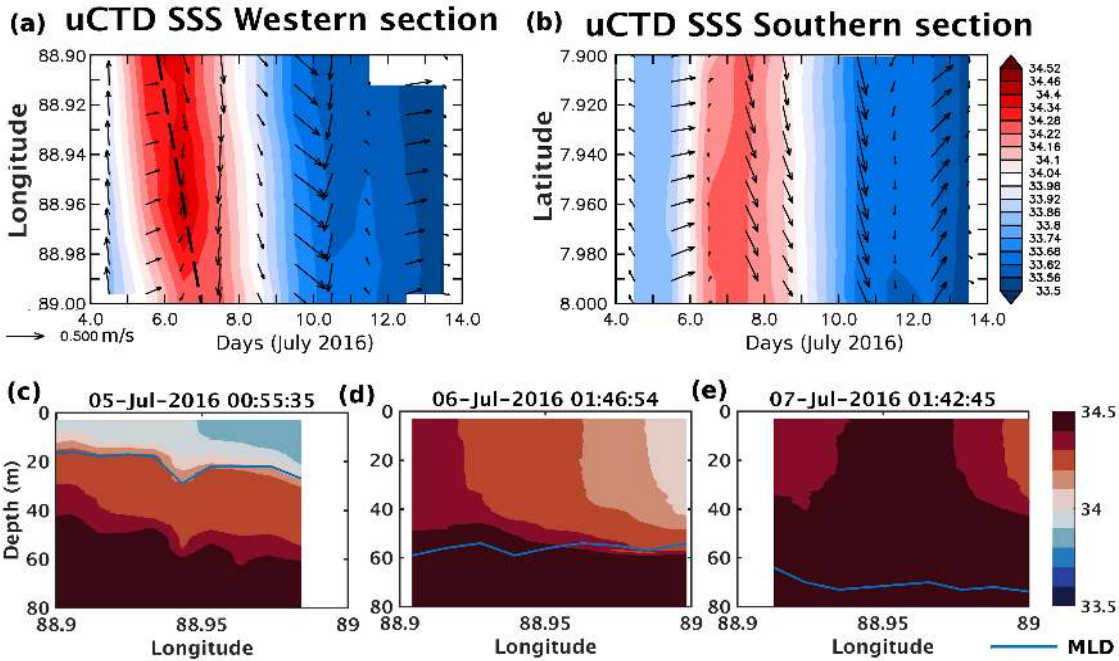
FIG. 8. Time series of: (a) uCTD surface salinity along the western section, (b) uCTD surface salinity along the southern section. The vectors represent the ADCP surface currents. Western uCTD salinity sections carried out on (c) 5 July, 2016 (d) 6 July, 2016 (e) 7 July, 2016. The thick blue line represent the mixed layer depth (MLD).
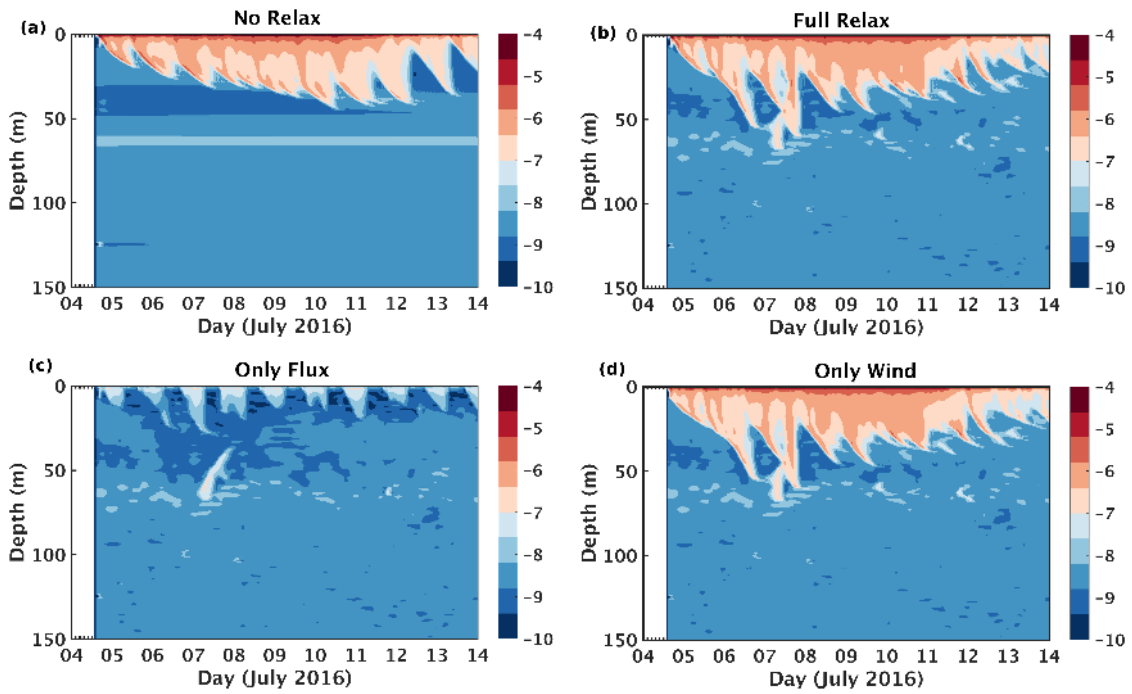
FIG. 9. Simulated $\log_{10} \varepsilon$ (W kg^{-1}) with GOTM experiments: (a) No Relax (b) Full Relax (c) Only Flux (d) Only Wind.
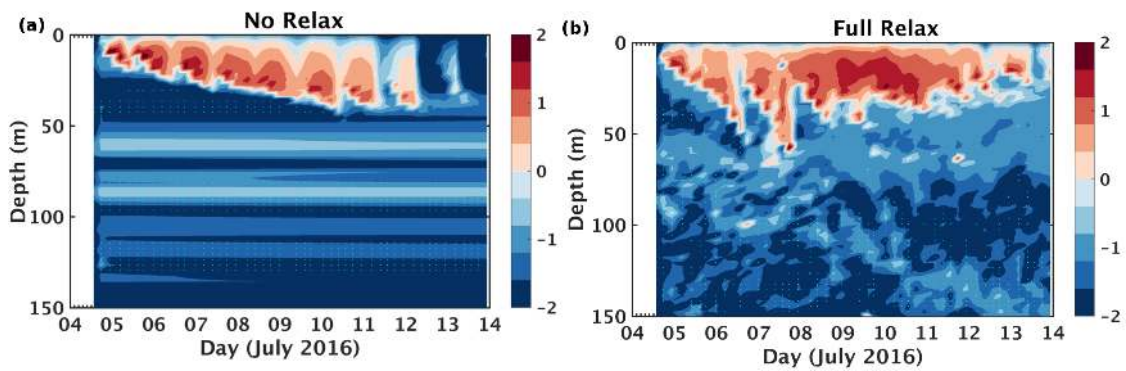
FIG. 10. Log$_{10}$ diapycnal salt flux (mg m^{-2} s^{-1}) calculated using the eddy diffusivity of salinity and vertical salinity gradient from the GOTM experiments: (a) No Relax, (b) Full Relax . The cyan dots indicates the region where the salt flux is downward.